RSC Advances

PAPER

View Article Online
View Journal | View Issue

Cite this: *RSC Adv.*, 2019, **9**, 2567

Template-free hydrothermal synthesis of $MgWO_4$ nanoplates and their application as photocatalysts†

Jie Meng, ‡ Tao Chen, ‡ Xiao Wei,* Jixue Li and Ze Zhang*

Received 8th August 2018
Accepted 3rd January 2019

DOI: 10.1039/c8ra06671j

rsc.li/rsc-advances

As a semiconductor, $MgWO_4$ has a potential in photocatalytic applications; however, it has been overlooked in previous studies; in this study, it has been demonstrated that $MgWO_4$ exhibits the ability to drive photocatalytic hydrogen evolution. Compared to nanoparticle structures, $MgWO_4$ nanoplates show an increased photocatalytic ability due to their higher specific surface area. Moreover, the formation mechanism of $MgWO_4$ nanoplates has been discussed. An oriented attachment and ripening process is proposed for the formation of the $MgWO_4$ nanoplates. This study demonstrates that $MgWO_4$ can be considered a valuable photocatalytic material, and future studies should be focused on how to promote its photocatalytic conversion efficiency.

Introduction

Magnesium tungstate ($MgWO_4$), known as a semiconductor with a wide band gap, has been extensively studied in various applications including luminescence, dielectric ceramics, catalysis, solid state lasers and so on.[1–4] $MgWO_4$ is currently of interest in the abovementioned fields due to the advantageous combination of light (Mg and O) and heavy (W) elements in its composition and the corresponding special structures.[5] As reported in previous studies, the optical band gap of $MgWO_4$ is about 4 eV with UV response.[4] Moreover, the bottom of the conduction band (CB) is lower than H^+/H_2 and the top of the valence band (VB) is higher than O_2/H_2O; this indicates that the photo-excited hole and electron pairs have enough energy to oxidize and reduce water, respectively.[3,6] However, to the best of our knowledge, $MgWO_4$ has remained unexplored in photocatalysis when compared with other compounds of the AWO_4 (A = Ca, Sr, Ba) family.[7,8]

Furthermore, as is well-known, the physical and chemical properties of semiconductors highly depend on their microstructures such as sizes, morphologies, crystal structures and so on.[9–12] Therefore, the desired properties could be obtained by rational control and design of the abovementioned parameters. In particular, explorations of two-dimensional (2D) nanoplates with novel structures contribute significantly to the evaluation of their possible roles in photocatalysis.[13,14] Furthermore, the plate-like or sheet-like structure may not only enhance the specific surface area but also suppress the recombination of photo-induced holes and electrons because these carriers can migrate from the interior to the surface more conveniently; this has been demonstrated in previous work.[15] Moreover, it would be beneficial to prepare plate-like structures through template-free and surfactant-free routes with low-cost and controllable synthesis processes. However, a $MgWO_4$ photocatalyst with a nanoplate structure has not yet been reported in previous literatures.

Hence, in this study, the $MgWO_4$ nanoplates were prepared by a facile hydrothermal reaction without any templates or surfactants. The formation process and possible mechanism of the $MgWO_4$ nanoplates have been discussed. Moreover, as a semiconductor, $MgWO_4$ has the ability to drive photocatalytic hydrogen evolution; this has been confirmed in this study. Compared with the nanoparticle structures, $MgWO_4$ nanoplates show an enhanced photocatalytic ability because of the higher specific surface area. This study demonstrates that $MgWO_4$ can be included in the family of photocatalysts, and the morphology of nanoplates provides a reference for the modification of other similar materials.

Results and discussion

Morphology and microstructure

The XRD pattern of the as-prepared $MgWO_4$ nanoplates after hydrothermal reaction for 12 h is displayed in Fig. 1b. All the diffraction peaks can be indexed to the tetragonal structure of $MgWO_4$ with a lattice constant of $a = b = 5.63$ Å and $c = 10.81$ Å; this is in agreement with the standard card (JCPDS no. 52-0390). Compared with the main peaks present in the standard pattern (Fig. 1a), the dominant diffraction peak in (003) indicates that the as-obtained samples may show a preferred orientation along the (001) planes; this has been further discussed

Center of Electron Microscopy, State Key Laboratory of Silicon Materials, School of Materials Science and Engineering, Zhejiang University, Hangzhou, 310027, PR China. E-mail: mseweixiao@zju.edu.cn; zezhang@zju.edu.cn; Fax: +86 571 87952797; Tel: +86 571 87952797

† Electronic supplementary information (ESI) available. See DOI: 10.1039/c8ra06671j

‡ These authors contributed equally to this work.

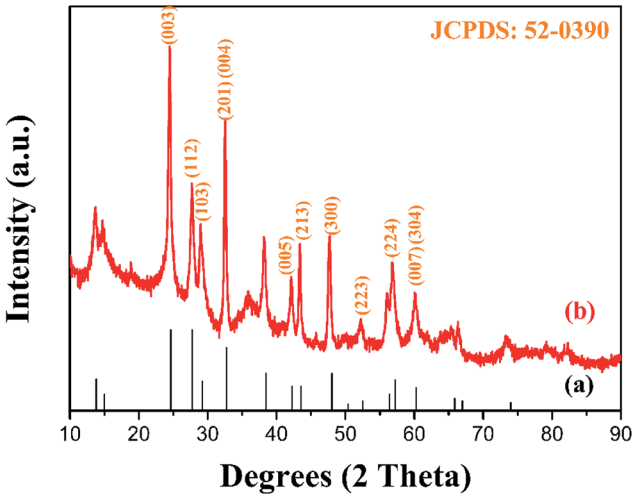

Fig. 1 XRD patterns of the (a) standard JCPDS card (52-0390) and (b) $MgWO_4$ nanoplates (12 h).

hereinafter *via* selected area electron diffraction (SAED) and high-resolution transmission electron microscopy (HRTEM) results.[10]

The SEM image of the as-obtained $MgWO_4$ nanoplates is shown in Fig. 2a. It can be seen that the $MgWO_4$ samples consist of plate-like nanostructures with an irregular shape (the thickness is about 45 nm). These plate-shaped structures were further confirmed by the transmission electron microscopy (TEM) image shown in Fig. 2b. Fig. 2c presents the selected area electron diffraction (SAED) pattern, and the three characteristic spots can be indexed to the diffraction planes of (003), (004) and (1/2 −1/2 0) for the tetragonal $MgWO_4$ phase. The interplanar spacing of about 0.363 nm is in agreement with the (003) facets in the corresponding high-resolution transmission electron microscopy (HRTEM) image (Fig. 2d). According to the SAED and HRTEM analysis, the exposed facets of $MgWO_4$ nanoplates are the (110) planes. The EDS spectrum (Fig. S1 and S2†) indicates that the $MgWO_4$ nanoplates are composed of Mg, W and O elements without other impurity phases, whereas the elements Cu and C result from the micro grid. To further study the surface chemical compositions and states of the $MgWO_4$ nanoplates, X-ray photoelectron spectroscopy (XPS) measurements were carried out, and the full range XPS spectrum and the corresponding high-resolution XPS spectra of Mg 1s, W 4f ($4f_{7/2}$: 34.5 eV and $4f_{5/2}$: 36.6 eV) and O 1s are shown in Fig. S3.† In the Mg 1s spectrum, we can find that the Mg oxidation states are mainly composed of +2, whereas the peak at 1302.9 eV may correspond to the existence of $Mg(OH)_2$.[16] The XPS results provide evidence of the existence of Mg^{2+} and W^{6+} on the surface of $MgWO_4$ nanoplates.[1,2,17]

Formation process

To better understand the formation process of the $MgWO_4$ nanoplates, the samples obtained at different hydrothermal reaction times were examined by TEM, SEM and XRD characterizations (Fig. 3 and S4†). At first, spherical nanoparticles were

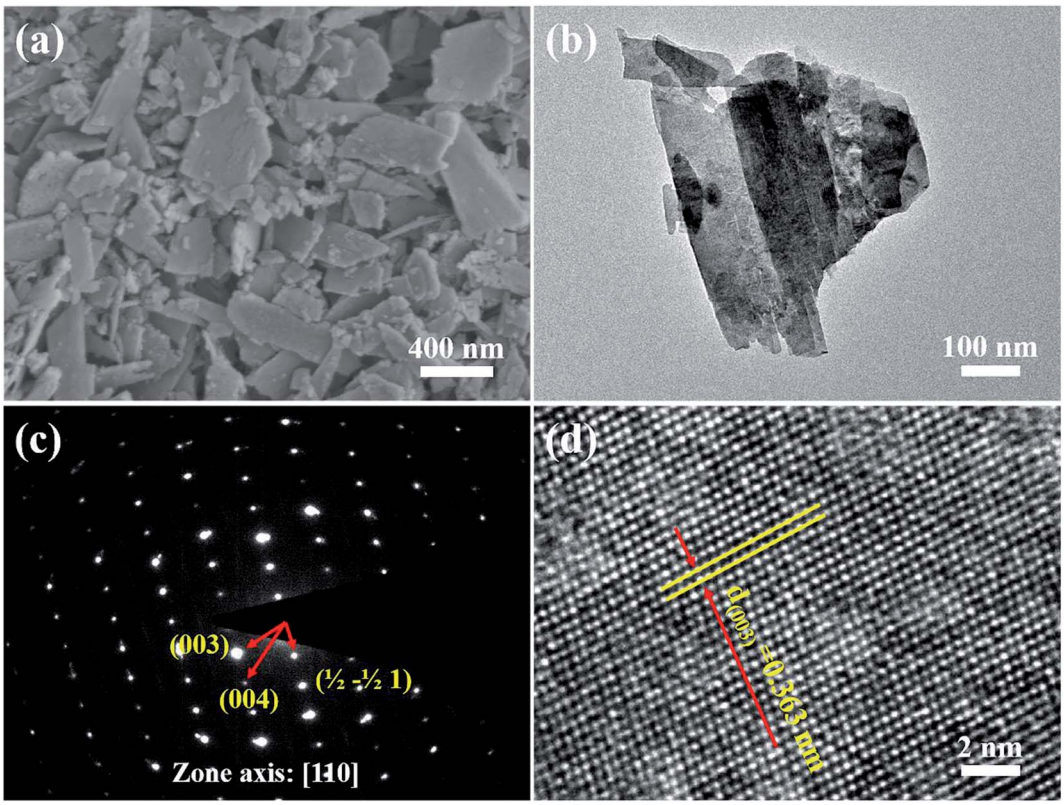

Fig. 2 Electron microscopy characterization of $MgWO_4$ nanoplates (12 h): (a) SEM image, (b) low magnification TEM image, (c) selective area electron diffraction (SAED) pattern and (d) high resolution TEM image.

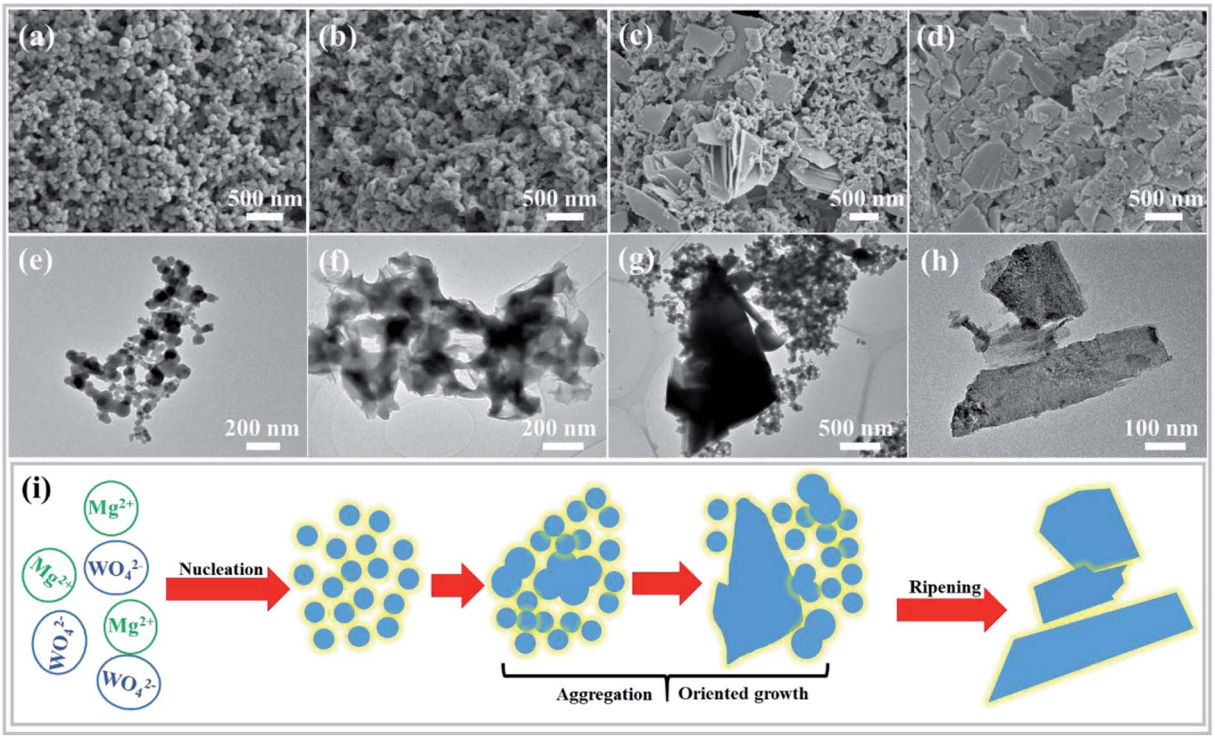

Fig. 3 Formation process of $MgWO_4$ nanoplates at different reaction times by SEM (a–d), TEM (e–h) characterizations and schematic (i) of $MgWO_4$ nanoplates: (a and e) 10 min, (b and f) 30 min, (c and g) 1 h and (d and h) 2 h.

formed after reaction for 10 min (Fig. 3a). Then, the primary nanoparticles tended to aggregate to produce the precursor of $MgWO_4$ nanoplates when time was prolonged to 30 min (Fig. 3b). When the reaction time reached 1 h, the nanoplates and nanoparticles are observed to co-exist, as shown in Fig. 3c. After hydrothermal treatment for 2 h and corresponding gradual ripening, the $MgWO_4$ nanoplates were constructed, as shown in Fig. 3d.

Based on the abovementioned morphology evolution, a rational formation mechanism was speculated, and the corresponding schematic can be seen in Fig. 3i. (i) Under the hydrothermal conditions, the reaction between Mg^{2+} and WO_4^{2-} starts in the mixed aqueous solution, and spherical particles are generated as a result of homogeneous nucleation.[18] (ii) The primary nanoparticles tend to aggregate to reduce the surface energy, and oriented attachment occurs between conjoined nanoparticles.[19,20] (iii) From the thermodynamic perspective, these two adjacent particles tend to share a common crystallographic orientation *via* rotation or fine-tuning.[21] In addition, the main framework of nanoplates is produced, and a crystallization process occurs, as confirmed by the XRD patterns (Fig. S4†). (iv) Finally, the $MgWO_4$ nanoplates are formed at the expense of the rest of the nanoparticles *via* an Ostwald ripening mechanism (Fig. S5†).[22,23]

Photocatalytic activity

The photocatalytic activities of the as-prepared $MgWO_4$ nanoplates were evaluated for hydrogen evolution under UV light irradiation. For comparison, $MgWO_4$ nanoparticles (Fig. S6 and S7†) were used as photocatalysts under the same experimental conditions. From the XPS valence band spectrum, it can be deduced that the valence band position is located at around 2 eV (Fig. S8†). Because the band gaps of $MgWO_4$ nanoparticles and nanoplates are estimated to 4.15 and 4.10 eV, respectively (Fig. 4c), the conduction band positions are about −2.15 and −2.10 eV, indicating that the photo-excited electrons have enough energy to reduce water (Fig. 5). As shown in Fig. 4a, both $MgWO_4$ samples exhibit photocatalytic activity; this implies that $MgWO_4$ can be a promising photocatalyst. In Fig. S9,† the $MgWO_4$ nanoplates do not show good stability in the recycling tests; this may be related to the photo-corrosion. Moreover, $MgWO_4$ nanoplates exhibited better photocatalytic performance than $MgWO_4$ nanoparticles, and their photocatalytic hydrogen evolution rate was about 1.35 times higher than that of $MgWO_4$ nanoparticles. It is known that the optical absorption range and the separation and migration efficiency are the main reasons impacting the final photocatalytic performance. To effectively study the possible mechanisms contributing to the differences in the photocatalytic rate, related characterizations were carried out, and the corresponding discussion have been provided hereinafter. The typical UV-vis diffuse reflectance spectra (DRS) of the as-prepared samples is displayed in Fig. 4c. The $MgWO_4$ samples with nanoplate shapes show a similar optical absorption ranges or edges with the nanoparticle structures. This indicates that the solar absorption range is not the key factor for the enhanced photocatalytic hydrogen evolution rate of $MgWO_4$ nanoplates. Therefore, photoluminescence

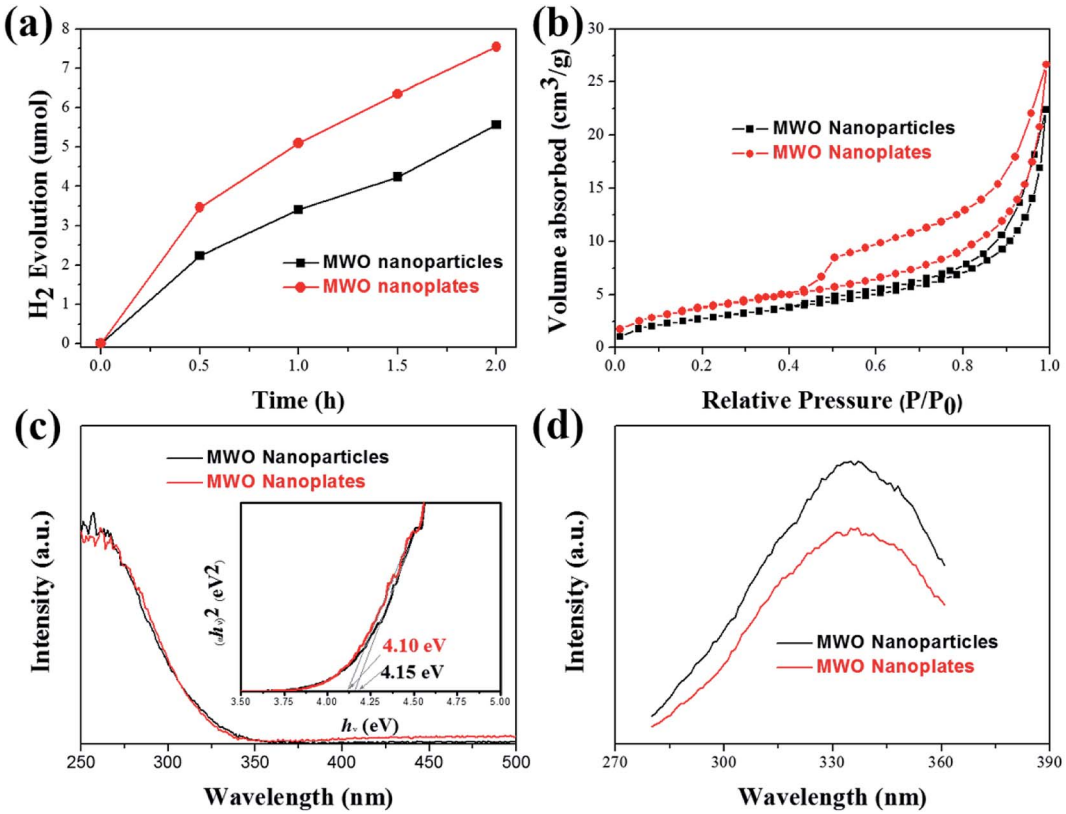

Fig. 4 (a) The photocatalytic hydrogen evolution, (b) N_2 adsorption–desorption curves, (c) UV-vis diffuse reflectance spectra (inset: the band gap determination by the Tauc method) and (d) PL spectra of $MgWO_4$ nanoplates (12 h).

(PL) emission spectra were obtained to characterize the recombination of photo-induced carriers. As shown in Fig. 4d, the strong emission peaks centered at about 335 nm could be ascribed to the band–band PL phenomenon of a photo-excited electron–hole; this was consistent with the DRS spectra.[24] In other words, the $MgWO_4$ nanoplates show a lower recombination rate of photo-induced carriers when compared with $MgWO_4$ nanoparticles. As observed from the Brunauer–Emmett–Teller (BET) nitrogen adsorption–desorption curves, the specific surface areas of the $MgWO_4$ nanoparticles and nanoplates are 10.46 and 14.05 $m^2\ g^{-1}$, respectively (Fig. 4b and Table S1†). The two samples show a typical IV isotherm, suggesting the presence of pores, which is consistent with the TEM analysis. Moreover, the corresponding H_2 production rates per surface area of the samples are almost the same (Fig. S10†). Therefore, the increased specific surface areas should be a key

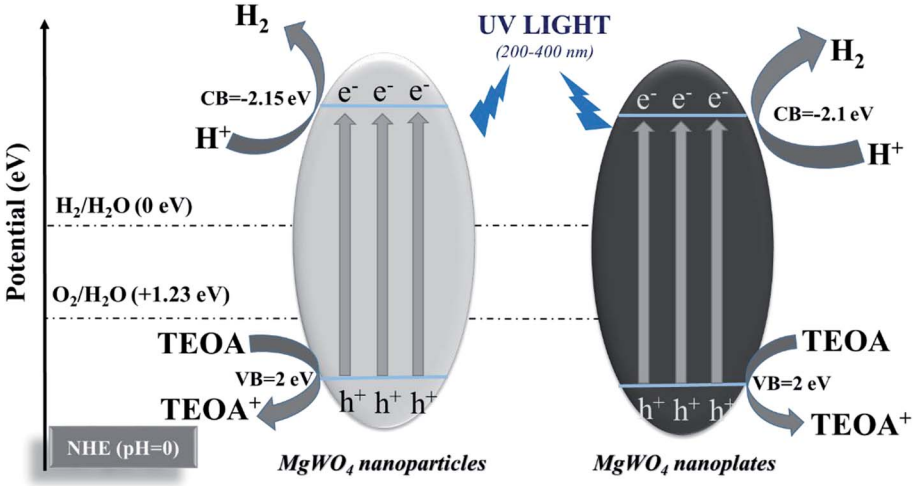

Fig. 5 Schematic of photocatalytic hydrogen evolution for $MgWO_4$ nanoparticles and $MgWO_4$ nanoplates (triethanolamine (TEOA) as a sacrificial agent).

factor for the enhanced photocatalytic activities of $MgWO_4$ nanoplates. As is well-known, a plate-like or sheet-like structure with high specific surface area can efficiently suppress the recombination of photo-induced carriers due to the short migration distance from the inner core to the surface; this is demonstrated in that the average particle size of $MgWO_4$ nanoparticles (72 nm) is larger than the average thickness of $MgWO_4$ nanoplates (45 nm). Furthermore, the high specific surface area is also beneficial for increasing the surface optical absorption and redox reaction area. Because of the larger specific surface area and corresponding efficient separation of photo-generated holes and electrons, the $MgWO_4$ nanoplates present a lower PL intensity, thus promoting the photocatalytic activity.

Conclusions

In summary, the $MgWO_4$ nanoplates were synthesized by a one-step hydrothermal reaction without any templates or surfactants. An oriented attachment and ripening process are proposed for the formation of the $MgWO_4$ nanoplates. As a semiconductor, $MgWO_4$ has the potential to participate in photocatalytic hydrogen evolution; this has been confirmed in this study. Compared with nanoparticle structures, $MgWO_4$ nanoplates show an increased photocatalytic ability as a result of their higher specific surface areas. This study demonstrates that $MgWO_4$ can be considered a viable photocatalyst, and future studies should be focused on how to promote its photocatalytic conversion efficiency.

Conflicts of interest

There are no conflicts to declare.

Acknowledgements

This work was supported by the National Natural Science Foundation of China (grant number: 11234011, 11327901, 51102208) and the Fundamental Research Funds for the Central Universities (2014QNA4008, 2017QNA4011).

Notes and references

1 J. Huang, B. Tian, J. Wang, Y. Wang, W. Lu, Q. Li, L. Jin, C. Li and Z. Wang, *CrystEngComm*, 2018, **20**, 608–614.
2 Y. Zu, Y. Zhang, K. Xu and F. Zhao, *RSC Adv.*, 2016, **6**, 31046–31052.
3 S. Wannapop, T. Thongtem and S. Thongtem, *Appl. Surf. Sci.*, 2012, **258**, 4971–4976.
4 P. D. Bhuyan, D. Singh, S. Kansara, P. Yadav, S. K. Gupta, Y. Sonvane, S. K. Rout and E. Sinha, *J. Mater. Sci.*, 2017, **52**, 4934–4943.
5 F. Danevich, D. Chernyak, A. Dubovik, B. Grinyov, S. Henry, H. Kraus, V. Kudovbenko, V. Mikhailik, L. Nagornaya and R. Podviyanuk, *Nucl. Instrum. Methods Phys. Res., Sect. A*, 2009, **608**, 107–115.
6 D. W. Kim, I.-S. Cho, S. S. Shin, S. Lee, T. H. Noh, D. H. Kim, H. S. Jung and K. S. Hong, *J. Solid State Chem.*, 2011, **184**, 2103–2107.
7 Z. Shan, Y. Wang, H. Ding and F. Huang, *J. Mol. Catal. A: Chem.*, 2009, **302**, 54–58.
8 C. Shivakumara, R. Saraf, S. Behera, N. Dhananjaya and H. Nagabhushana, *Mater. Res. Bull.*, 2015, **61**, 422–432.
9 T. Chen, J. Meng, S. Wu, J. Pei, Q. Lin, X. Wei, J. Li and Z. Zhang, *J. Alloys Compd.*, 2018, **754**, 184–189.
10 G. Xi and J. Ye, *Chem. Commun.*, 2010, **46**, 1893–1895.
11 M. Long, W. Cai, Z. Wang and G. Liu, *Chem. Phys. Lett.*, 2006, **420**, 71–76.
12 J. Meng, X. Fu, K. Du, X. Chen, Q. Lin, X. Wei, J. Li and Z. Zhang, *Int. J. Hydrogen Energy*, 2018, **43**, 9224–9232.
13 H. Zhang, J. Yang, D. Li, W. Guo, Q. Qin, L. Zhu and W. Zheng, *Appl. Surf. Sci.*, 2014, **305**, 274–280.
14 H. Wang, J. Gao, T. Guo, R. Wang, L. Guo, Y. Liu and J. Li, *Chem. Commun.*, 2012, **48**, 275–277.
15 S. Xie, Y. Wang, Q. Zhang, W. Deng and Y. Wang, *Chem. Commun.*, 2015, **51**, 3430–3433.
16 C. Liu, Y. Xin, X. Tian and P. K. Chu, *Thin Solid Films*, 2007, **516**, 422–427.
17 A. Katrib, F. Hemming, P. Wehrer, L. Hilaire and G. Maire, *J. Electron Spectrosc. Relat. Phenom.*, 1995, **76**, 195–200.
18 Y. Mi, Z. Huang, F. Hu, Y. Li and J. Jiang, *J. Phys. Chem. C*, 2009, **113**, 20795–20799.
19 R. L. Penn and J. F. Banfield, *Science*, 1998, **281**, 969–971.
20 J. F. Banfield, S. A. Welch, H. Zhang, T. T. Ebert and R. L. Penn, *Science*, 2000, **289**, 751–754.
21 H. Xu, W. Wang and L. Zhou, *Cryst. Growth Des.*, 2008, **8**, 3486–3489.
22 W. Yang, F. Gao, G. Wei and L. An, *Cryst. Growth Des.*, 2009, **10**, 29–31.
23 Y. Sun, B. Mayers and Y. Xia, *Nano Lett.*, 2003, **3**, 675–679.
24 J. Meng, J. Pei, Z. He, S. Wu, Q. Lin, X. Wei, J. Li and Z. Zhang, *RSC Adv.*, 2017, **7**, 24097–24104.